Zaniuk V.
PhD student

Gurskyi V.
Doctor of Technical Sciences, Professor

Lviv Polytechnic National University

Занюк В.С.
аспірант

Гурський В.М.
д.т.н. професор

Національний університет "Львівська політехніка"

УДК 621.01
DOI: 10.37128/2306-8744-2026-1-19

DYNAMIC ANALYSIS AND DESIGN OF A VIBRATORY FINISHING DEVICE FOR BIONIC PROSTHETIC HAND COMPONENTS

The aim of this study is to develop and investigate a vibratory machine with a toroidal bowl intended for post-processing polymer components of bionic prosthetic devices manufactured using additive manufacturing technologies. A design of a laboratory vibratory installation is proposed, in which the toroidal geometry of the working bowl is used to ensure the formation of a closed spiral trajectory of motion of the abrasive media and processed parts.

To analyze the operation of the device, a mathematical model of spatial oscillations of the vibrating system was developed, in which the working bowl is considered as a rigid body with six degrees of freedom, taking into account the action of the unbalanced excitation drive, elastic suspension, and damping. Numerical solution of the system of differential equations of motion was performed in the Maple environment, which made it possible to obtain time dependencies of the center-of-mass displacements and to study the spatial nature of the oscillations.

To verify the adequacy of the mathematical model, spatial trajectories of a characteristic point located on the mean radius of the torus were constructed for different separation angles of the unbalances. The obtained results demonstrated the possibility of controlling the spatial character of the oscillatory motion and forming operating modes required for the circulating movement of the working media in the toroidal bowl.

For the first time, the use of a toroidal bowl in a vibratory finishing machine for post-processing bionic prosthetic components with the realization of a closed spiral trajectory as the working path has been substantiated. An approach for verifying the dynamic model of the vibratory machine by analyzing the trajectories of a characteristic point obtained from the numerical solution of the equations of motion in the Maple environment has been proposed.

Key words: *vibratory finishing machine, toroidal bowl, bionic prosthesis, additive manufacturing.*

Introduction. The development of additive manufacturing technologies has opened new opportunities for producing functional components of bionic upper-limb prostheses. Multi Jet Fusion (MJF) and Selective Laser Sintering (SLS) technologies have become widely used for manufacturing parts with high strength comparable to injection-molded plastic products [1], good geometric stability, and biocompatibility [2].

However, surfaces of such parts exhibit characteristic roughness and grain structure, which limits their use in final medical devices without additional post-processing. As a result, the surface of prosthetic elements that actively interact with the external environment tends to wear rapidly: it becomes scratched, loses its initial smoothness, and acquires an unattractive appearance after relatively short use (Fig. 1). Traditional mechanical polishing or grinding methods are often ineffective for parts with complex geometries, especially prosthetic fingers, which are not only small in size and composed of multiple interconnected elements but also represent the most functionally loaded

parts of the prosthetic structure that constantly interact with surrounding objects.

One effective solution to this problem is the use of vibratory finishing machines. Such equipment can uniformly polish surfaces due to the controlled motion of abrasive media and can ensure process automation with minimal human intervention. At the same time, their application for post-processing parts manufactured by 3D printing remains insufficiently studied, which determines the relevance of research in this field.

Fig. 1. Allbionics TR bionic prosthetic hand showing visible signs of surface wear after use

Therefore, the development of a specialized vibratory machine with design features suitable for post-processing bionic prosthetic fingers in small-batch production is relevant. It is proposed to use a toroidal bowl, which makes it possible to implement a closed spiral trajectory of motion of both the processed parts and the abrasive media. Such geometry creates conditions for more uniform and controlled surface processing. The oscillatory motion of the bowl is generated by an unbalanced excitation drive that produces the required forces and moments.

In this context, the objective of this work is to develop and investigate a vibratory machine with a toroidal bowl intended for surface finishing of small components of bionic prostheses manufactured using additive technologies. To achieve this objective, the study includes the development of a mathematical model of the motion trajectory of the parts, engineering calculations of the main structural elements, and verification of the system operation using Maple.

The developed device represents a laboratory prototype intended for further experimental investigation of the influence of vibratory finishing on the surface quality of parts manufactured by MJF and SLS technologies. At the same time, most requirements typical for industrial machines (such as energy efficiency, durability of components, maintenance convenience, noise level, and productivity) are not considered in this work, since they do not directly affect the surface processing results. The presented results are aimed at substantiating the conceptual design of the vibratory device and creating a basis for further experimental studies.

Literature Review. In modern prosthetics, polymer materials produced using additive manufacturing technologies are increasingly used, particularly polyamide 12 (PA12), which is characterized by good mechanical properties, stability in humid environments, and biocompatibility. Several studies report that PA12 manufactured using Multi Jet Fusion (MJF) technology is non-toxic, insoluble in water, and does not undergo degradation in humid environments [2]. However, it has also been noted that this material does not possess antibacterial properties and may be susceptible to biofilm formation, which creates the need for additional post-processing, including polishing or chemical smoothing.

The effectiveness of PA12 for medical applications and prosthetics has also been confirmed in a number of studies [3–8]. For example, in the rapid manufacturing of individualized prosthetic sockets, PA12 was identified as the most suitable material compared to polycarbonate and ABS [3]. Similar results are presented in other review papers emphasizing that MJF and SLS technologies are already widely used for manufacturing medical devices and prosthetic components [4], [5]. In [7], the development of a lightweight finger prosthesis manufactured from PA12 using MJF technology is presented, demonstrating the suitability of this material for small functional prosthetic components due to its favorable combination of strength and low weight.

However, one of the key unresolved problems for PA12 components produced by SLS and MJF technologies remains the high surface roughness. According to [9], even when compared with FFF printing, the surface roughness of SLS parts remains high, although it is approximately 43% lower. When comparing properties of SLS parts with injection-molded components, it was shown that the strength is comparable, but SLS parts are more brittle and exhibit significantly rougher surfaces [1]. This feature limits the use of such parts without additional post-processing in mechanical assemblies and medical devices where low surface roughness and smooth surfaces are required [10].

For this reason, many studies focus on the development of effective post-processing methods for additive manufacturing technologies [10–15]. In [11], the influence of different post-processing methods (mechanical treatment, chemical treatment, and antibacterial coatings) on the surface properties of PA12 manufactured by SLS and MJF technologies was investigated. It was found that SLS samples had, on average, a surface roughness approximately 33% higher than that of MJF samples. Mechanical treatment reduced the arithmetic mean height parameter (Sa) by 42%, while chemical treatment reduced it by 80%. A decrease in surface slope parameters (Sdq) and developed surface area ratio (Sdr) resulted in improved gloss and optical quality of the surface. Regarding antibacterial coatings based on silver, one type had almost no influence on the surface properties, whereas another produced a slight smoothing effect.

Another study [15] evaluated three types of mechanical post-processing of SLS-printed parts: grinding, diamond turning, and milling. Grinding showed the best results, achieving a surface roughness of Ra = 0.055 μm (a reduction of 99.2%) and demonstrating the highest quality and stability of results. Diamond turning achieved Ra = 0.28 μm (–96.1%), while milling resulted in Ra = 0.45 μm (–93.6%). All methods slightly reduced the hardness of the material by 0.13%, 1.42%, and 2.46%, respectively.

Laser polishing is another effective post-processing technique capable of significantly improving surface quality. According to [14], surface roughness was reduced by 91%, reaching a minimum Ra value of 0.6 μm. At the same time, the physical properties of the parts remained almost unchanged: hardness did not change, while tensile strength decreased by only about 6%. Such polishing also improved the tribological properties of the surface, which opens prospects for the use of polished PA12 parts in medical and sealing application.

Some studies also indicate potential long-term stability issues of polymer materials. In [12], the mechanical and aesthetic stability of PA12 components after 12 months of operation was investigated. It was found that SLS samples retained nearly unchanged strength (≈45 → 43 MPa, i.e., –4%), while MJF samples lost approximately 34% of their strength (43 → 29 MPa). In the case of SLS, coloring slightly increased strength after 12 months (44 → 45 MPa), while for MJF it only partially slowed degradation (31 MPa compared to 28 MPa for uncolored samples). As a result, SLS (PA2200) demonstrated significantly higher resistance to physical degradation compared with MJF (PA12), where the strength reduction approached 50%.

Thus, despite the widespread use of additive manufacturing technologies in medicine, surface quality and durability of polymer components remain significant challenges, stimulating the development of alternative post-processing methods. One such method is vibratory finishing, which allows simultaneous polishing of a large number of parts with complex geometries. In [16], it was shown that the use of chemical accelerators in the vibratory finishing process reduced the processing time of hard steel components from 48 hours to 4 hours, achieving a surface roughness of Ra = 1–2 μinch. This demonstrates the potential for adapting vibratory finishing technology to polymer components.

Recent studies on modeling vibratory finishing processes demonstrate significant progress in the simulation of media motion. Works [17–20] show that simulation systems based on RecurDyn–EDEM, ABAQUS/Explicit, and ADAMS–EDEM can reliably reproduce the trajectories of particles in toroidal bowls, opening possibilities for optimization and validation of vibratory machine designs. In particular, [17] confirms that such simulations show only minor deviations from experimental data, while [18] demonstrates that ANSYS CFX can be used to determine the distribution of surface roughness on complex three-dimensional surfaces after processing. Additionally, [21] proposes modeling the working media of vibratory machines as non-Newtonian fluids, providing an alternative approach to analyzing particle motion and complementing DEM-based studies of complex flows in toroidal bowls.

Fundamental theoretical principles and practical recommendations for vibratory machines with toroidal bowls are most comprehensively described in domestic sources [22], where the principles of harmonic oscillations of working bodies and engineering calculation methods are presented in detail. These works form the theoretical basis for further research and design of modern vibratory systems, including the system proposed in this study.

Presentation of the main material. The trajectory of motion of the abrasive media and

processed parts in a toroidal bowl has a complex spatial character, which can be approximately described as a closed spiral developing on the surface of a torus. Such a motion pattern ensures cyclic movement of particles along the annular channel, continuous renewal of contact zones between the parts and the media, and minimal direct contact between the parts themselves. This, in turn, contributes to a more uniform grinding and polishing process.

To describe the dynamics of the toroidal bowl, it is considered as a rigid body with six degrees of freedom. The adopted coordinate system of the oscillatory system is shown in Fig. 2a. The generalized vector of coordinates has the following form:

$$\mathrm{q} = [x, y, z, \varphi, \theta, \psi] \quad (1)$$

where x, y, z are the linear displacements of the center of mass, and φ, θ, ψ are the small rotation angles of the bowl with respect to the corresponding axes.

The equations of motion of the entire system can be logically divided into three main parts. The system of equations describing the linear motion of the center of mass is written as:

$$\begin{cases} m\ddot{x} + c_x\dot{x} + k_x x = F_x, \\ m\ddot{y} + c_y\dot{y} + k_y y = F_y, \\ m\ddot{z} + c_z\dot{z} + k_z z = F_z. \end{cases} \quad (2)$$

The system of equations describing the angular motion of the bowl is:

$$\begin{cases} J_\varphi\ddot{\varphi} + c_\varphi\dot{\varphi} + k_\varphi\varphi = M_x, \\ J_\theta\ddot{\theta} + c_\theta\dot{\theta} + k_\theta\theta = M_y, \\ J_\psi\ddot{\psi} + c_\psi\dot{\psi} + k_\psi\psi = M_z. \end{cases} \quad (3)$$

where m is the mass of the oscillating part including the attached mass of the load; $J_\varphi, J_\theta, J_\psi$ are the principal central moments of inertia about the corresponding axes; c_i and k_i $(i = x, y, z, \varphi, \theta, \psi)$ are the equivalent damping and stiffness coefficients corresponding to the generalized coordinates; F_x, F_y, F_z and M_x, M_y, M_z are the components of generalized excitation forces and moments.

In addition, to describe the motion of the entire oscillatory system, the rotation of the unbalanced excitation drive (Fig. 2b) is taken into account and is represented by the equation of moments [23–25]:

$$J\ddot{\alpha} + \mathrm{c}_\alpha\dot{\alpha} + M_b + V = M_d, \quad (4)$$

where α is the rotation angle of the shaft; J is the reduced moment of inertia of the unbalance shaft; k_α is the torsional damping coefficient; M_d is the torque of the electric motor; M_b is the friction torque in the bearings; V is the vibratory torque.

The variation of the motor torque is described by the relation [24]:

$$M_d = \frac{2M_{max}s_m\left(\frac{\omega - \dot{\alpha}}{\omega}\right)}{{s_m}^2 + \left(\frac{\omega - \dot{\alpha}}{\omega}\right)^2}, \quad (5)$$

where $M_{max} = \frac{2.2P}{\omega}$ is the maximum motor torque; $s_m = 0.15$ is the slip of the electric motor; ω is the synchronous angular velocity.

The vibratory torque acting on the motor shaft is expressed as:

$$V(t) = m_d r_d \cdot (\ddot{y}cos\alpha - \ddot{x}sin\alpha) + m_d r_d\left(\ddot{y}cos(\alpha + \gamma) - \ddot{x}sin(\alpha + \gamma)\right) \quad (6)$$

where m_d is the mass of the unbalance; r_d is the distance from the shaft axis to the center of mass of the unbalance and γ – is the separation angle of the unbalances.

The friction torque in the bearings is assumed in the following form:

$$M_b = f\frac{m_d r_d \dot{\alpha}^2 d}{2}, \quad (7)$$

where f – is the friction coefficient in the bearings and d is the bearing diameter.

In the adopted coordinate system, the components of excitation forces are expressed as:

$$\begin{cases} F_x = 2m_d r_d \dot{\alpha}^2 \cos\left(\frac{\gamma}{2}\right)\cos\left(\alpha + \frac{\gamma}{2}\right), \\ F_y = 2m_d r_d \dot{\alpha}^2 \cos\left(\frac{\gamma}{2}\right) sin\left(\alpha + \frac{\gamma}{2}\right), \\ F_z(t) = 0; \end{cases} \quad (8)$$

$$\begin{cases} M_x = 2m_d r_d \dot{\alpha}^2 h_d \sin\left(\frac{\gamma}{2}\right) cos\left(\alpha + \frac{\gamma}{2}\right), \\ M_y = 2m_d r_d \dot{\alpha}^2 h_d \sin\left(\frac{\gamma}{2}\right) sin\left(\alpha + \frac{\gamma}{2}\right), \\ M_z = 0, \end{cases} \quad (9)$$

where h_d is the distance between the planes of the unbalance locations along the shaft axis.

Design Calculations. To determine the structural parameters of the unbalanced excitation drive, the design oscillation amplitudes are preliminarily assumed as follows: linear amplitude X = 1 mm and angular amplitude Φ = 0.007 rad. These values are used in the calculation based on the known relationships presented in [22].

The amplitude values of the excitation force and moment required to ensure the specified oscillation amplitudes of the container are determined according to the following relations:

$$F_0 = mX\omega^2; \; M_0 = J_\varphi \Phi\omega^2. \quad (10)$$

Since the unbalances are spaced along the rotor axis at a distance h_d, the required amplitude values of the inertial force of a single unbalance and the separation angle between the unbalances are determined from the relations:

$$F_{in} = \frac{1}{2h_d}\sqrt{F_0^2 {h_d}^2 + 4M_0^2}; \quad (11)$$

$$\gamma = arccos\left(\frac{F_0^2 {h_d}^2 - 4M_0^2}{F_0^2 {h_d}^2 + 4M_0^2}\right). \quad (12)$$

The required static moment of a single unbalance is determined by the expression:

$$m_d r_d = \frac{F_{\text{ін}}}{\omega^2}. \quad (13)$$

The power of the electric motor required to ensure a harmonic oscillation regime is estimated using the generalized relation:

$$P = \frac{\sqrt{6}\omega^3}{2\eta}\left(mX^2 + J_\psi \Phi^2\right) \quad (14)$$

where η is the motor efficiency.

According to the calculation results, an asynchronous electric motor with a rated power of 180 W was selected. Structurally, an unbalance with a mass of 0.24 kg and an eccentricity of 0.04 m was adopted, providing the required static moment.

In the design of a vibratory machine with a toroidal bowl, one of the key elements is the vibration isolation system, which provides elastic suspension of the container and determines the character of its spatial oscillations. The most appropriate solution is the use of helical cylindrical springs as vibration isolators, which are widely available and have a broad range of standard sizes.

In vibratory machines of this type, the springs operate under a complex stress–strain state. Because the upper end of the spring is attached to the container performing spatial oscillations and the lower end is fixed to the stationary supporting structure, the spring simultaneously experiences compression, bending, and torsion.

The total stiffness of the vibration isolation system in different directions can be determined using the corresponding relations [26]. The axial stiffness (along the spring axis) is defined as:

$$k_z = \frac{G d_s^4 n_s}{8 D_c^3 N_c}. \quad (15)$$

The transverse stiffness (spring bending in the X and Y planes) is defined as:

$$k_x = k_y = \frac{12 E J_s n_s}{\left[N_c\left(t_0 - \frac{8QD_c^3}{n_s G d_s^4}\right)\right]^3 \frac{2+\sigma\cos\tau}{2\sin\tau}}. \quad (16)$$

The angular stiffness around the vertical axis of the bowl is determined as:

$$k_\psi = \frac{12 E J_s R_0^2 n_s}{\left[N_c\left(t_0 - \frac{8QD_c^3}{n_s G d_s^4}\right)\right]^3 \frac{2+\sigma\cos\tau}{2\sin\tau}}. \quad (17)$$

The angular stiffness during bowl tilting is determined as:

$$k_\theta = k_\varphi = \frac{12 E J_s n_s Z_k^2}{\left[N_c\left(t_0 - \frac{8QA_c^3}{n_s G d_s^4}\right)\right]^3 \frac{2+\sigma cos\ \tau}{2sin\ \tau}} + \frac{G d_s^4 R_0}{8\Omega_c^3 N_c}, \quad (18)$$

where E, G, σ are the Young's modulus, shear modulus and Poisson's ratio of the spring material, respectively;

d_s, D_c, J_s are the wire diameter, mean coil diameter and second moment of area of the spring wire cross-section of the spring, respectively; n_S is the number of springs; Q is the weight of the oscillating system; N_c is the number of active coils; t_0 is the pitch of the spring in the free state; τ is the helix angle of the spring coil; R_0 is the radius at which the springs are mounted; Z_k is the distance from the center of mass to the lower mounting plane of the springs.

For the elastic suspension of the working bowl, six identical cylindrical springs made of spring steel were selected (E = 207 GPa; G = 80 GPa; σ = 0.29). All geometric and structural parameters of the suspension are presented in Table 1.

Table 1.

Parameters of the elastic suspension

Parameter	Symbol	Value	Units
Spring wire diameter	d	1.25	*mm*
Mean coil diameter	D	10	*mm*
Number of active coils	N_C	5	
Spring pitch	t_0	5.45	*mm*
Helix angle of the spring	τ	10	*deg*
Second moment of area of the wire cross-section	J_s	9.6×10^{-14}	m^4
Number of springs in the suspension	n_S	6	
Radius of spring arrangement	R_0	120	*mm*
Distance from center of mass to mounting plane	Z_k	130	*mm*

coordinate is introduced through the relative damping ratio ξ. For translational coordinates, the damping coefficients are determined as:

$$c_i = 2\xi\sqrt{m k_i}.\ i \in \{x, y, z\} \quad (19)$$

For rotational coordinates:

$$c_j = 2\xi\sqrt{J_j k_j}, \qquad j \in \{\varphi, \theta, \psi\} \quad (20)$$

where J_j represents the corresponding reduced moments of inertia; k_i and k_j are the corresponding stiffness coefficients.

Based on the calculated stiffness and mass–inertial parameters (Fig. 3), the natural frequencies of the oscillatory system were determined as: $f_{0x} = f_{0y} = 9.40$ Hz, $f_{0z} = 7.40$ Hz, $f_{0\varphi} = f_{0\theta} = 15.5$ Hz, $f_{0\psi} = 8.34$ Hz. The operating frequency of the system is $f = \omega/2\pi \approx 23.9$ Hz, which exceeds all natural frequencies of the system. Therefore, the installation operates in a super-resonant regime, and resonance phenomena do not occur within the operating range.

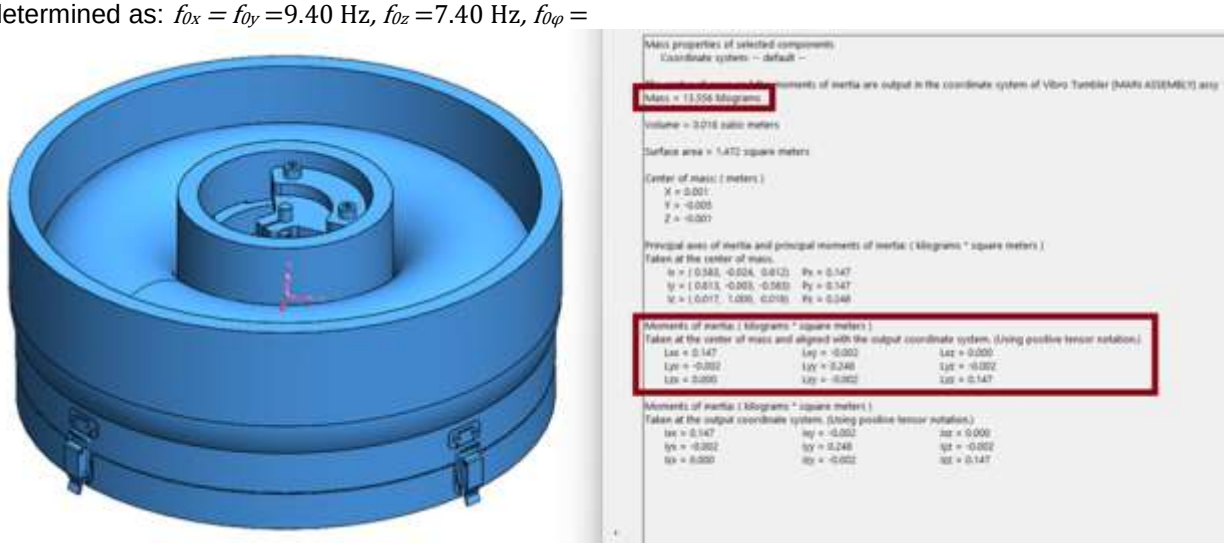

Fig. 3. Mass–inertial characteristics of the oscillating part of the vibratory machine taking into account the attached mass of the load

Table 2.

Calculated parameters of the mathematical model of the vibratory machine

Parameter	Symbol	Value	Units
Mass of the oscillating part	m	13.55	*kg*
Moment of inertia	J_φ	0.14678	*kg·m²*
	J_θ	0.14678	*kg·m²*
	J_ψ	0.24755	*kg·m²*
Stiffness (15-18)	k_x, k_y	47261	*N/m*
	k_z	29296	*N/m*
	k_φ, k_θ	1384	*N·m /rad*
	k_ψ	680	*N·m /rad*
Damping (19-20)	c_x, c_y	325	*N·s/m*
	c_z	256	*N·s/m*
	c_φ, c_θ	5	*N·m·s/rad*
	c_ψ	5	*N·m·s/rad*
Unbalance mass (13)	m_d	0.3	*kg*
Distance from shaft axis to the center of mass of the unbalance	r_d	0.03	*m*
Distance between unbalances along the shaft axis	h_d	0.18	*m*
Mean radius of the bowl	R_t	0.135	*m*
Angular velocity of the shaft	ω	150	*rad/s*
Drive power (14)	P	180	*W*
Bearing diameter	d	0.02	*m*
Friction coefficient in bearings	f	0.004	
Drive damping coefficient	c_α	0.001	

Mathematical Modeling. The developed mathematical model of the oscillatory system is presented as a system of second-order differential equations (2–4) with constant coefficients and harmonic excitation.

To obtain the time dependencies of the displacements in generalized coordinates, the system of equations was reduced to a Cauchy problem by specifying zero initial conditions for the coordinates and their first derivatives. The

numerical solution of the Cauchy problem was carried out by direct integration of the system of differential equations in the Maple environment, which made it possible to obtain continuous time-domain solutions for the oscillatory system.

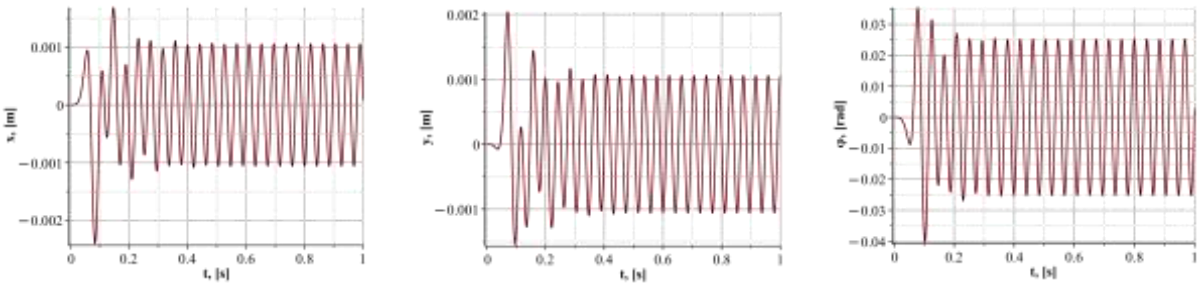

Fig. 4. Time dependence of the displacement of the center of mass of the vibratory system along the x and y axes and the bowl tilt angle φ (at γ=90).

Figure 4 shows the time dependence of the displacement of the system center of mass along the horizontal axes and the tilt angle of the bowl about one of these axes. The plot demonstrates the harmonic nature of oscillations with a frequency determined by the angular velocity of rotation of the unbalances and a constant amplitude defined by the mass–inertial characteristics, stiffness, and damping parameters of the oscillatory system.

The increased amplitudes observed at the initial section of the graph are caused by the presence of a free component of the solution that arises when zero initial conditions are specified under non-zero harmonic excitation. As the oscillations progress, the influence of this component gradually decreases due to damping, and the system transitions to a steady-state periodic regime with constant amplitude. The steady-state oscillation amplitude of the center of mass is approximately $A_x \approx 1$mm.

Since equation (4) describing the drive was included in the mathematical model, it was also possible to obtain the corresponding time dependencies of the drive parameters. The graphs demonstrate a short transient process during system start-up. At the initial stage, the motor torque (Fig. 5a) increases to its maximum value, accelerating the system, after which it decreases and stabilizes at a level sufficient to maintain the steady operating regime. Accordingly, the angular velocity quickly reaches the operating value and then remains nearly constant (Fig. 5b).

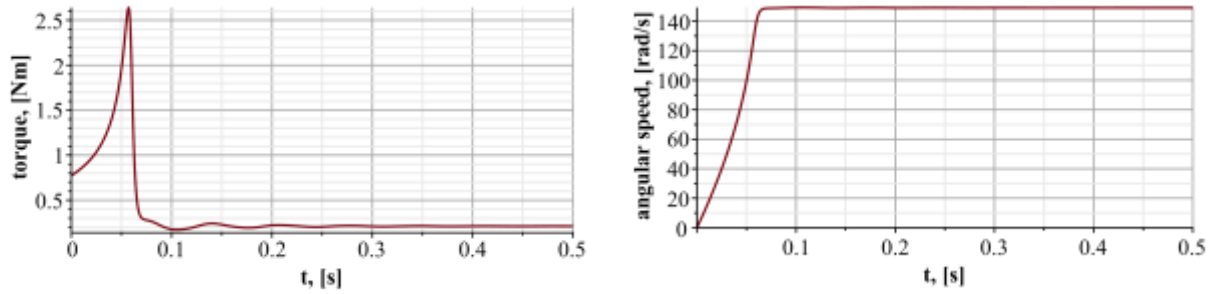

a) ***b)***

Fig. 5. Time dependencies of the drive parameters of the vibratory system: (a) - motor torque; (b) - angular speed of unbalance rotation

Trajectory Analysis. The construction of the spatial trajectory of a point located on the mean radius of the toroidal bowl is used as a criterion for verifying the adequacy of the proposed mathematical model of oscillatory motion and for determining the vertical component of the oscillations. The agreement between the obtained trajectory and the expected physical behavior of the vibratory system confirms the correctness of the mathematical model.

The position of a point located on the mean radius R_t (Fig. 2), rigidly connected to the body, in the global coordinate system is determined by the relation:

$$r_P(t) = r_{CM}(t) + R(t)r_{R_t}, \qquad (21)$$

where $r_{CM}(t)$ is the position vector of the center of mass; $R(t)$ represents the elementary Euler rotation matrices; r_{R_t} is the constant radius vector of the point in the coordinate system attached to the bowl.

To analyze the spatial character of motion, a point located on the mean radius of the torus was selected, for which:

$$r_{R_t} = [R_t \quad 0 \quad 0]^T \qquad (22)$$

Substituting this vector into the expression for $r_{CM}(t)$ makes it possible to obtain the parametric equations describing the coordinates of the point:

$$\begin{cases} P_x(t) = x(t) + R_x r_{R_t}, \\ P_y(t) = y(t) + R_y r_{R_t}, \\ P_z(t) = z(t) + R_z r_{R_t}. \end{cases} \qquad (23)$$

Using the obtained parametric curve (23), the trajectory of motion of the point R_t can be constructed in the Maple environment for different separation angles of the unbalances. In the case where no separation between the unbalances is present (Fig. 6a), the trajectory takes the form of a closed almost planar curve close to a circle. This indicates the dominance of the horizontal component of the oscillatory motion generated by the excitation forces and the absence of angular oscillations.

For intermediate values of the separation angle (Fig. 6b, d–f), the trajectory transforms into a spatial elliptical curve, which indicates the presence of both horizontal and vertical components of oscillatory motion and the formation of a combined spatial motion required to generate the spiral movement of the abrasive media along the bowl.

When the unbalances are separated in opposite directions (Fig. 6c), the trajectory becomes a complex spatial curve with pronounced curvature lying in one of the vertical planes. This is caused by the presence of only angular oscillations generated by excitation moments.

It is also observed that at the separation angle γ=270° (Fig. 6.f), an elliptical trajectory with an opposite inclination is formed compared with the case γ=90°. This indicates a change in the direction of motion of the point and, consequently, a change in the direction of circulation of the working media inside the bowl.

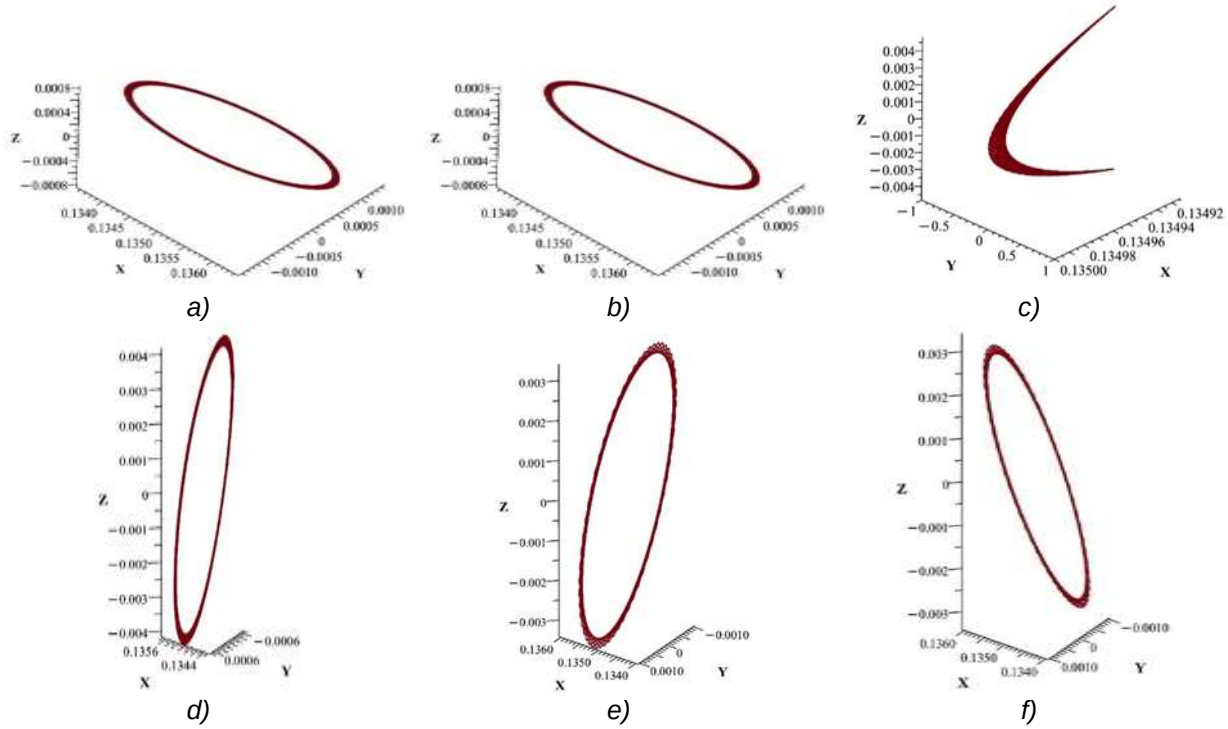

Fig. 6. Trajectories of motion of a point on the mean radius of the torus for different separation angles of the unbalances: a - *γ*=0°; b - *γ*=20°; c - *γ*=180°, d - *γ*=120°; e - *γ*=90°; f - *γ*=270°.

Table 3.

Amplitude values of oscillations of a point on the mean radius of the torus for different separation angles of the unbalance

Separation angle of unbalances, *γ*	A_{X1}, mm	A_{Y1}, mm	A_{Z1}, mm
0°	1.5	1.5	0
20°	1.47	1.47	0.81
90°	1.06	1.06	3.41
120°	0.75	1.75	4.18
180°	0.04	0	4.82
270°	1.06	1.06	3.41

Device Design. The developed design of the device is shown in Fig. 7. The working toroidal bowl (1) is mounted on a base plate (2). A distinctive feature of the design is the quick-release mounting

of the bowl (10), which allows rapid unloading of the bowl without dismantling additional structural elements or performing complex manipulations.

The oscillatory motion of the bowl is generated by a central drive unit consisting of a shaft (6) and two unbalances (4). The shaft is driven by an electric motor (7) through a flexible coupling (8). All elements are mounted on the supporting frame of the device (9). The working bowl (1) is installed on a vibration isolation suspension using elastic elements (3), which provide the required compliance of the system and allow the system to pass through resonance during start-up.

One of the critical structural elements of the vibratory machine is the shaft on which the unbalances are mounted. To verify its strength, a stress–strain analysis was performed using the finite element method in SolidWorks Simulation (Fig. 8). The loading was applied in the form of a centrifugal load, taking into account the unbalances and the operating angular velocity ω.

The calculations were performed for characteristic separation angles of the unbalances, and the obtained maximum stress values are summarized in Table 4.

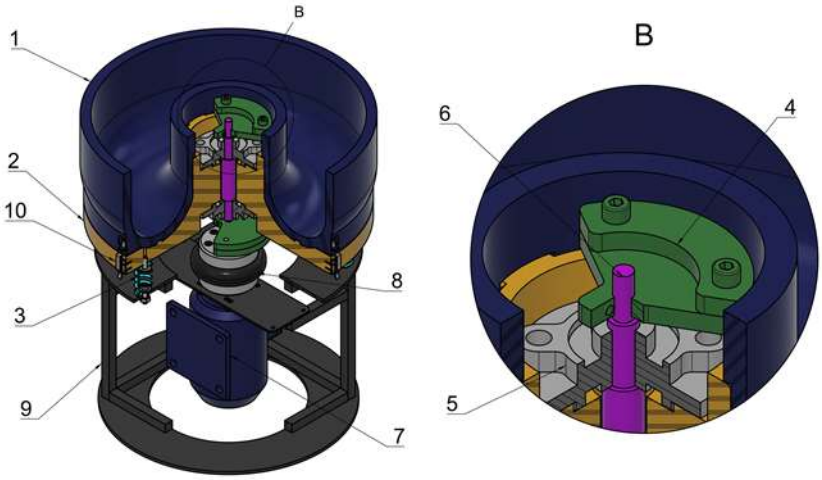

Fig. 7. Structural diagram of the vibratory device with a toroidal bowl.

Table 4.

Stresses in the drive shaft at characteristic separation angles of the unbalances

Separation angle, *γ*	Parameter	
	Maximum equivalent stress (von Mises), *MPa*	Safety factor relative to yield strength
0°	59.8	3
90°	61.4	2.9
180°	62	2.9

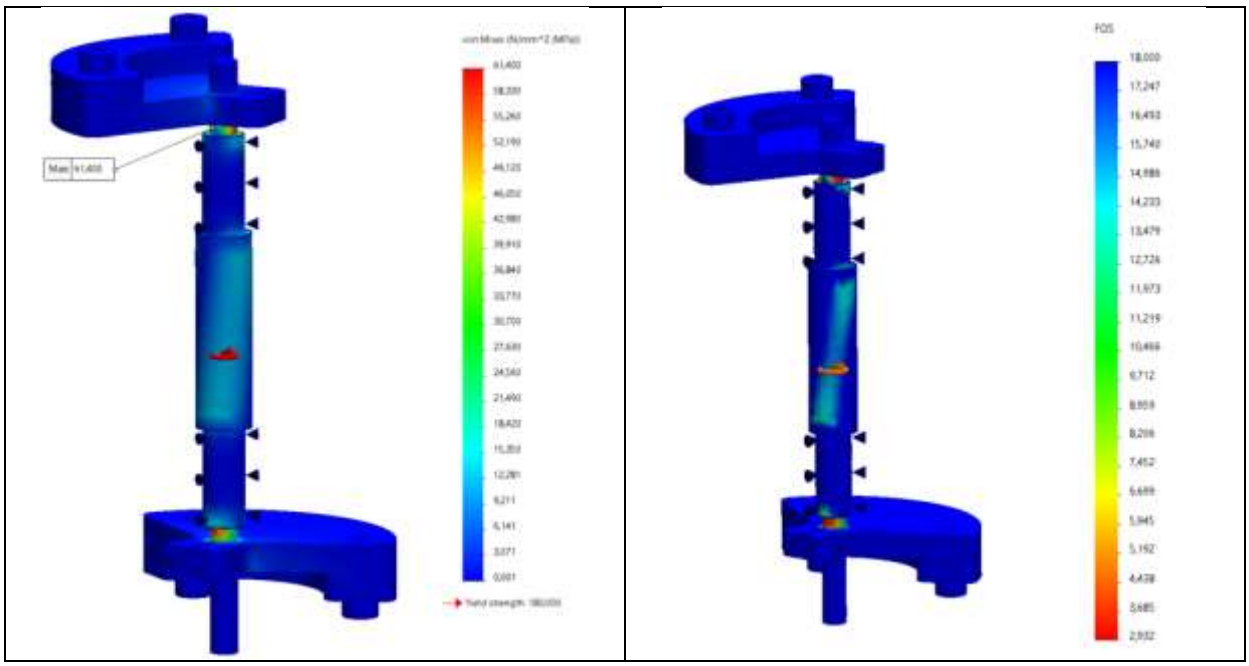

a)	b)

Fig. 8. Results of the stress–strain analysis of the drive shaft in SolidWorks Simulation (γ = 90°): (a) equivalent von Mises stress distribution; (b) factor of safety (FOS)

The maximum equivalent stresses in all investigated operating regimes do not exceed 62 MPa, which is significantly lower than the yield strength of the material (approximately 180 MPa). The minimum safety factor is about n ≈ 2.9, confirming sufficient strength of the drive shaft within the entire range of characteristic separation angles of the unbalances.

Conclusions. A laboratory vibratory machine with a toroidal bowl for finishing polymer components of bionic prosthetic devices manufactured using additive technologies (MJF, SLS) has been proposed. A distinctive feature of the design is the quick-release toroidal bowl, which simplifies unloading and operation of the installation. It is shown that the use of a toroidal geometry of the working element ensures the formation of a spatial spiral trajectory of motion of the abrasive media and processed parts.

A mathematical model of spatial oscillations of the vibratory system has been developed, in which the working bowl is considered as a rigid body with six degrees of freedom, taking into account the action of the unbalanced excitation drive, elastic suspension, and damping. Numerical solution of the system of differential equations in the Maple environment made it possible to obtain the time dependencies of the center-of-mass displacements and the trajectory of motion of a point located on the mean radius of the bowl. It has been shown that variation of the separation angle of the unbalances allows control of the spatial character of the oscillatory motion and enables the formation of operating regimes required for circulating movement of the media in the toroidal bowl. This adjustment provides variation of the oscillation amplitudes of the point on the mean radius of the torus within the ranges A_{x1} = 0-1.5 mm, A_{y1} = 0-1.75 mm and A_{z1} = 0-4.82 mm, which makes it possible to modify the spatial structure of media motion within the working zone.

The parameters of the unbalanced excitation drive and the elastic suspension of the oscillatory system have been determined. Finite element analysis of the stress–strain state of the drive shaft showed that the maximum equivalent stresses do not exceed allowable values, while the safety factor is approximately 2.9. The proposed device can be used as a laboratory installation for further experimental investigations of vibratory finishing processes, including studies employing DEM modeling to determine optimal operating regimes.

References

1. Van Hooreweder, B., Moens, D., Boonen, R., Kruth, J.-P., & Sas, P. (2013). On the difference in material structure and fatigue properties of nylon specimens produced by injection molding and selective laser sintering. Polymer Testing, 32(5), 972–981. https://doi.org/10.1016/j.polymertesting.2013.04.014

2. Priyadarshini, B. M., Kok, W. K., Dikshit, V., Feng, S., Li, K. H. H., & Zhang, Y. (2022). 3D printing biocompatible materials with Multi Jet Fusion for bioreactor applications. International Journal of Bioprinting, 9(1), 623. https://doi.org/10.18063/ijb.v9i1.623

3. Górski, F., Wichniarek, R., Kuczko, W., Żukowska, M., & Suszek, E. (2020). Rapid manufacturing of individualized prosthetic sockets. Advances in Science and Technology Research Journal, 14(1), 42–49. https://doi.org/10.12913/22998624/113425

4. Turek, P., Budzik, G., Oleksy, M., & Bulanda, K. (2020). Polymer materials used in medicine processed by additive techniques. Polimery, 65(7–8), 510–515. https://doi.org/10.14314/polimery.2020.7.2

5. Salmi, M. (2021). Additive manufacturing processes in medical applications. Materials, 14(1), 191. https://doi.org/10.3390/ma14010191

6. Khorasani, M., et al. (2024). Multi Jet Fusion (MJF) of polymeric components: A review of process, properties and opportunities. Additive Manufacturing, 91, 104331. https://doi.org/10.1016/j.addma.2024.104331

7. Ryu, W., Choi, Y., Choi, Y. J., & Lee, S. (2020). Development of a lightweight prosthetic hand for patients with amputated fingers. Applied Sciences, 10(10), 3536. https://doi.org/10.3390/app10103536

8. Zakręcki, A., Cieślik, J., Bazan, A., & Turek, P. (2024). Innovative approaches to 3D printing of PA12 forearm orthoses: A comprehensive analysis of mechanical properties and production efficiency. Materials, 17(3), 663. https://doi.org/10.3390/ma17030663

9. Terekhina, S., Tarasova, T., Egorov, S., Guillaumat, L., & Hattali, M. L. (2020). On the difference in material structure and fatigue properties of polyamide specimens produced by fused filament fabrication and selective laser sintering. The International Journal of Advanced Manufacturing Technology, 111(1–2), 93–107. https://doi.org/10.1007/s00170-020-06026-x

10. Kantaros, A., Ganetsos, T., Petrescu, F., Ungureanu, L., & Munteanu, I. (2024). Post-

production finishing processes utilized in 3D printing technologies. Processes, 12(3), 595. https://doi.org/10.3390/pr12030595

11. Bazan, A., Turek, P., & Zakręcki, A. (2023). Influence of antibacterial coating and mechanical and chemical treatment on the surface properties of PA12 parts manufactured with SLS and MJF techniques in the context of medical applications. Materials, 16(6), 2405. https://doi.org/10.3390/ma16062405

12. Zakręcki, A., & Cieślik, J. (2025). Influence of ageing and post-processing on the mechanical and aesthetic stability of PA12-based 3D-printed components for medical devices. Materials, 18(19), 4478. https://doi.org/10.3390/ma18194478

13. Johansson, I. (2020). Post-processing for roughness reduction of additive manufactured polyamide 12 using a fully automated chemical vapor technique (Master's thesis, KTH Royal Institute of Technology). https://urn.kb.se/resolve?urn=urn:nbn:se:kth:diva-279316

14. Eckhardt, L., et al. (2023). Laser beam polishing of PA12 parts manufactured by powder bed fusion. Lasers in Manufacturing and Materials Processing, 10(4), 563–585. https://doi.org/10.1007/s40516-023-00213-w

15. Rohrsen, N. C., & Hagedorn, D. (2024). Improving the surface quality of additive manufactured polyamide parts using conventional treatment methods. The International Journal of Advanced Manufacturing Technology, 132(5–6), 2347–2358. https://doi.org/10.1007/s00170-024-13279-3

16. Nebiolo, W. P. (n.d.). Vibratory bowl optimization by proper mechanical set-up and the use of chemical accelerators to virtually eliminate hand polishing of steel parts. In SUR/FIN Proceedings. National Association for Surface Finishing (NASF).

17. Liu, W., Wang, S., Jiang, Q., Morgan, M., & Liu, X. (2022). Study on the motion characteristics of abrasive media in vibratory finishing. Journal of Physics: Conference Series, 2198(1), 012035. https://doi.org/10.1088/1742-6596/2198/1/012035

18. Wan, S., Fong, W. S., & Tay, Z. H. (2010). Process modelling and simulation of vibratory finishing of fixtured components.

19. Kang, Y. S., Hashimoto, F., Johnson, S. P., & Rhodes, J. P. (2017). Discrete element modeling of 3D media motion in vibratory finishing process. CIRP Annals, 66(1), 313–316. https://doi.org/10.1016/j.cirp.2017.04.092

20. Wang, X., Yang, S., Li, W., & Wang, Y. (2018). Vibratory finishing co-simulation based on ADAMS–EDEM with experimental validation. The International Journal of Advanced Manufacturing Technology, 96(1–4), 1175–1185. https://doi.org/10.1007/s00170-018-1639-0

21. Silman, T., & Domblesky, J. (2007). Investigation of workload fluid characteristics in vibratory finishing. In SUR/FIN Proceedings. National Association for Surface Finishing (NASF).

22. Lanets, O. Osnovy rozrakhunku ta konstruiuvannia vibratsiinykh mashyn. Knyha 1. Teoriia ta praktyka stvorennia vibratsiinykh mashyn z harmoniinym rukhom robochoho orhana. Lviv: Vydavnytstvo Lvivskoi politekhniky. 2008. 620. [in Ukrainian].

23. Gurskyi, V., Korendiy, V., Krot, P., Zimroz, R., Kachur, O., & Maherus, N. (2023). On the dynamics of an enhanced coaxial inertial exciter for vibratory machines. Machines, 11(1), 97. https://doi.org/10.3390/machines11010097

24. Yaroshevich, N., Gursky, V., Puts, V., Yaroshevych, O., & Martyniuk, V. (2022). On the dynamics of vibrational capture of rotation of an unbalanced rotor. Vibroengineering Procedia, 42, 1–6. https://doi.org/10.21595/vp.2022.22413

25. Yaroshevich, N., Yaroshevych, O., & Lyshuk, V. (2021). Drive dynamics of vibratory machines with inertia excitation. In J. M. Balthazar (Ed.), Vibration engineering and technology of machinery (Vol. 95, pp. 37–47). Springer. https://doi.org/10.1007/978-3-030-60694-7_2

26. Yaroshenko, L. V., & Slobodianyk, A. D. (2025). Elastic suspensions of vibrating machines with adjustable electromechanical drive. Vibration Engineering and Technology of Machinery, 3(118), 45–54. https://doi.org/10.37128/2306-8744-2025-3-5

ДИНАМІЧНИЙ АНАЛІЗ ТА ПРОЕКТУВАННЯ ВІБРАЦІЙНОГО ПРИСТРОЮ ДЛЯ ФІНІШНОЇ ОБРОБКИ ДЕТАЛЕЙ БІОНІЧНИХ ПРОТЕЗІВ РУКИ

Метою цього дослідження є розроблення та дослідження вібраційної машини з тороїдальною робочою ємністю, призначеної для фінішної обробки полімерних компонентів біонічних протезних пристроїв, виготовлених за допомогою адитивних технологій. Запропоновано конструкцію лабораторної вібраційної установки, у якій тороїдальна геометрія робочої ємності використовується для забезпечення формування замкненої спіральної траєкторії руху абразивного середовища та оброблюваних деталей.

Для аналізу роботи пристрою розроблено математичну модель просторових коливань вібраційної системи, у якій робоча ємність розглядається як тверде тіло з шістьма ступенями вільності з урахуванням дії дебалансного приводу збудження, пружної підвіски та демпфування.

Чисельне розв'язання системи диференціальних рівнянь руху виконано в середовищі Maple, що дало змогу отримати часові залежності переміщень центра мас і дослідити просторовий характер коливань.

Для перевірки адекватності математичної моделі побудовано просторові траєкторії характерної точки, розташованої на середньому радіусі тора, для різних кутів рознесення дебалансів. Отримані результати продемонстрували можливість керування просторовим характером коливального руху та формування робочих режимів, необхідних для циркуляційного переміщення робочого середовища в тороїдальній ємності.

Уперше обґрунтовано використання тороїдальної робочої ємності у вібраційній фінішній машині для обробки компонентів біонічних протезів із реалізацією замкненої спіральної траєкторії як робочого шляху. Запропоновано підхід до перевірки динамічної моделі вібраційної машини шляхом аналізу траєкторій характерної точки, отриманих на основі чисельного розв'язання рівнянь руху в середовищі Maple.

Ключові слова: *вібраційна машинка для обробки, тороїдальна чаша, біонічний протез, адитивне виробництво.*

Відомості про авторів

Gurskyi Volodymyr, Doctor of Technical Sciences, Professor in the Department of Robotics and Integrated Mechanical Engineering Technologies at Lviv Polytechnic National University, Lviv, Ukraine, email: Volodymyr.M.Hurskyi@lpnu.ua , https://orcid.org/0000-0002-7141-0280
Zaniuk Vitaliy, postgraduate student at the National University "Lviv Polytechnic**".**

Гурський Володимир Миколайович, доктор технічних наук, професор кафедри робототехніки та інтегрованих технологій машинобудування Національного університету "Львівська політехніка", м.Львів, Україна, email: Volodymyr.M.Hurskyi@lpnu.ua , https://orcid.org/0000-0002-7141-0280
Занюк Віталій Сергійович, аспірант Національного університету "Львівська політехніка".

Стаття надійшла 11.03.2026
Стаття прийнята 20.03.2026
Опубліковано 17.04.2026